




One-sided destructive quantum interference from an exceptional-point-based metasurfaceHong Liang ^{1,2} Kai Ming Lau ^{1,2} Wai Chun Wong,^{1,2} Shengwang Du,³ Wing Yim Tam,¹ and Jensen Li ^{1,2,*}¹*Department of Physics, The Hong Kong University of Science and Technology, Clear Water Bay, Kowloon, Hong Kong, China*²*IAS Center for Quantum Technologies, The Hong Kong University of Science and Technology, Clear Water Bay, Hong Kong, China*³*Department of Physics, The University of Texas at Dallas, Richardson, Texas 75080, USA*

(Received 22 July 2021; revised 16 November 2021; accepted 7 December 2021; published 21 December 2021)

We propose the concept of one-sided destructive quantum interference based on lossy metasurfaces. It corresponds to one-sided beam splitting with 50:25:0 in percentage ratio among the transmission and the two reflection efficiencies, which can be realized by a metasurface with unidirectional zero reflection (UZR) from a non-Hermitian exceptional point. When two identical photons enter both sides of the lossy metasurface, quantum interference only occurs for the single-photon output state towards one side but not the other due to UZR. Such one-sided quantum interference can be further made totally destructive. This effect along with UZR provides more degrees of freedom in quantum interference control and entangled states construction.

DOI: [10.1103/PhysRevA.104.063710](https://doi.org/10.1103/PhysRevA.104.063710)**I. INTRODUCTION**

Metasurface, a thin layer of nanostructures array, is useful for miniaturizing conventional optical elements, with applications ranging from beam steering and lensing to vortex beam structuring, holograms, and combinations of these functions [1–3]. On the other hand, metasurfaces can also be used as a flexible platform to study exotic phenomena, such as topological photonics and non-Hermitian physics [4,5]. The developments in the past decade in non-Hermitian photonics have found that the material loss, in competition with coupling between different parts of the system, can become useful to generate an exceptional point: the coalescence of both the eigenvalues and eigenvectors of the system Hamiltonian or the response matrix [6,7]. It then gives rise to a series of counterintuitive wave phenomena, as examples, in loss-induced transmission [8], unidirectional zero reflection (UZR) [9], enhanced sensing [10], and lasing-mode selection [11]. Recently, exceptional points have been demonstrated using metamaterials [12,13] and metasurfaces at the optical frequencies [14–16]. UZR can be used as a signature of a non-Hermitian exceptional point of the scattering matrix of metasurfaces [9,17,18].

In the quantum optics regime, tailor-made metasurfaces have already been found useful in simplifying quantum tomography [19], and generating entanglement for spins and orbital angular momenta [20–22], etc. While unitary operations in quantum optics are constructed conventionally from a network of common optical components such as beam splitters and wave plates [23–26], metasurfaces allow us to design tailor-made unitary transformations for miniaturization. For example, arbitrary $U(2)$ operations and single-photon two-qubit $U(4)$ operations can be realized using dielectric metasurfaces [27]. Furthermore, lossy metasurfaces, as a

manifestation of non-Hermitian systems, also play an important role to extend conventional quantum optical operations to nonunitary transformations. For example, lossy metasurfaces can tune quantum interference from destructive to constructive [28]. It is interesting to note that while the concept of a non-Hermitian exceptional point has an origin in quantum theory [6,7], it was first realized in classical optical systems, and then, in quantum optical systems recently [29–31]. To further exploit the non-Hermitian properties of metasurfaces in quantum optical operations, we would like to investigate the role of exceptional points in manipulating two-photon quantum interference.

In this work, by treating a metasurface as a two-port device, extending from a beam splitter in conventional quantum operations, we propose a design of a lossy bianisotropic metasurface exhibiting a one-sided two-photon quantum interference effect. When two indistinguishable photons enter both sides of the metasurface capturing UZR, quantum interference only exists for single-photon output state on one side but not the other side. This asymmetric interference effect comes from the broken mirror symmetry of the metasurface along the light propagation which gives zero reflection coefficient on one side but nonzero on the other. Furthermore, the quantum interference can be further tuned to totally destructive by controlling the transmission and reflection amplitudes of the metasurface.

II. THEORY AND RESULTS

A two-photon quantum interference effect for a two-port device can be visualized by an input-output map in Fock states, as shown in Fig. 1. Each square cell, labeled by its input state (column) and output state (row), is colored red (solid cell) for generally nonzero values, blue (horizontal lines) for zero from destructive quantum interference, and white for zero from conservation of energy. Each input or output Fock state is represented by two indices with the first (second)

*Corresponding author: jensenli@ust.hk

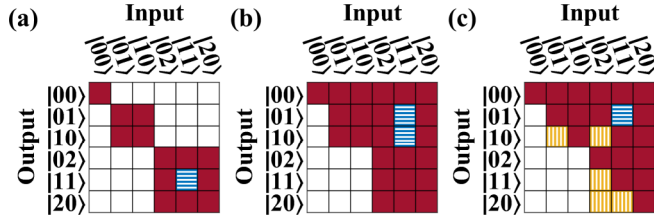


FIG. 1. Quantum interference for a two-port device. (a) HOM effect from a lossless 50:50 beam splitter: $|11\rangle$ input state is forbidden to transfer to $|11\rangle$ output due to destructive quantum interference indicated as blue color (horizontal lines). The white color denotes zero transfer probabilities due to conservation of energy while the red color (solid cell) denotes generally nonzero values. (b) Apparent nonlinear absorption from a lossy system: $|11\rangle$ input state is forbidden to transfer to the single-photon states $|01\rangle$ and $|10\rangle$, but not the states with zero or two photons. (c) One-sided destructive quantum interference from a metasurface. $|11\rangle$ input state is forbidden to transfer to $|01\rangle$ state because of quantum destructive interference but the single-photon output state $|10\rangle$ cannot be tuned as quantum interference is missing due to a designed UZR. The UZR also induces zero probabilities for processes where the number of photons in port 1 is increased, indicated by the yellow cells (vertical lines).

index indicating the number of photons in port 1(2). For the Hong-Ou-Mandel (HOM) effect [32], the two ports are for lossless 50:50 beam splitting, and the process $|11\rangle \rightarrow |11\rangle$ is forbidden [blue horizontal lines in Fig. 1(a)], which results from two-photon destructive quantum interference. In another case, when loss is added to the system, Fig. 1(b) shows the case of apparent nonlinear absorption enabled by a 25:25 beam splitter [33–37]. For a two-photon input state $|11\rangle$, the probabilities for only one photon survives, $|10\rangle$ and $|01\rangle$, are both zero, i.e., either both photons are absorbed or neither. Such a loss-induced quantum interference effect has been recently extended to plasmonic systems and metasurfaces whose scattering matrix can now be tailor-made to achieve constructive quantum interference [28,38].

Now, we discuss the proposed one-sided quantum interference effect, schematically illustrated in Fig. 1(c). For a $|11\rangle$ input, we would like the quantum interference to occur only on one side to get a destructive interference at the single-photon output state $|01\rangle$ (blue horizontal lines) while the quantum interference is turned off at the output state $|10\rangle$. Here, normal incidence from the front (back) side of a metasurface is defined as input port 1(2) while its transmitted light is defined as the corresponding output port [see Fig. 2(a)]. As we shall see, such one-sided quantum interference is enabled by a proper design of metasurface with UZR so that the backward reflection coefficient (r_b) is zero. It is worthwhile to note that an immediate consequence of the UZR is the zero probabilities for $|01\rangle \rightarrow |10\rangle$ and other processes with the number of photons in port 1 being increased [yellow vertical lines in Fig. 1(c)] since the additional photons have to come from input port 2 with nonzero backward reflection.

Figure 2(b) shows a unit cell of our proposed bianisotropic metasurfaces located at $z = 0$. Each unit cell in a square lattice consists of two vertical gold bars with separation h , lengths l_1 and l_2 , widths w_1 and w_2 , and is driven into resonance by incident light polarized along the y direction. Full-wave

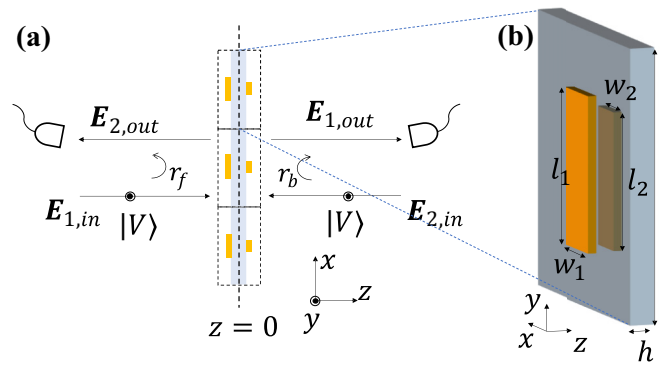


FIG. 2. (a) Proposed experiment with a bianisotropic metasurface. $E_{1,in}$ ($E_{2,in}$) denotes the E field, polarized along y direction, at input port 1(2). Subscript “out” is used for E fields at output ports. (b) A square unit cell of metasurface with periodicity 300 nm consists of two vertical gold bars (thickness 20 nm) with dimensions $l_2 = 150$ nm, and $w_2 = 50$ nm while l_1 , w_1 , and separation h will be swept in later designs. Drude model for the permittivity of gold: $\epsilon = 9 - f_p^2 / (f^2 + i\gamma_p f)$ with $f_p = 2180$ THz, $\gamma_p = 16.2$ THz.

simulations (CST Studio Suite) are performed to obtain the classical response at each frequency, as a 2×2 scattering matrix $S = \begin{pmatrix} t_f & r_b \\ r_f & t_b \end{pmatrix}$ where $t_f = t_b = t$ for reciprocity and $r_f \neq r_b$ for the broken mirror symmetry along the z direction. The subscript “ f ” (“ b ”) stands for the forward (backward) incidence. We scan l_1 (length of the front bar) and h (separation between the two bars) with other dimensions listed in the caption of Fig. 3 and w_1 (80 nm) is fixed. In Fig. 3(a), we plot the positions of UZR, $|r_b| \cong 0$ at a resonance dip, as a black curve in the parameter space. The UZR condition equivalently means coalesce of both eigenvalues and eigenvectors for S (termed as a non-Hermitian exceptional point hereafter). When h decreases, l_1 has to increase in obtaining a larger loss contrast to balance the stronger coupling between the two gold bars to get an exceptional point and thus UZR [18]. Figure 3(b) shows the $|t|$, $|r_f|$, and $|r_b|$ frequency spectra for the case $(l_1, h) = (191 \text{ nm}, 16 \text{ nm})$, denoted by a star in Fig. 3(a),

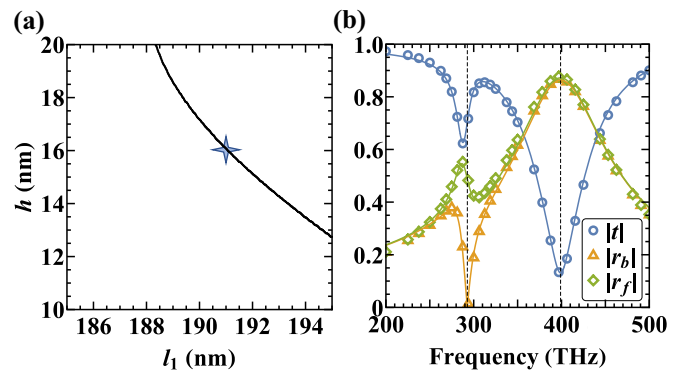


FIG. 3. Locations of UZR in the phase space l_1 - h as the black curve in (a) with w_1 fixed at 80 nm. The star indicates the case with $(l_1, h) = (191 \text{ nm}, 16 \text{ nm})$ with their frequency spectra for $|t|$, $|r_f|$, and $|r_b|$, shown in (b). Symbols (solid lines) are the full-wave simulation (coupled-mode theory) results. UZR occurs at around 293 THz.

showing clearly the UZR occurs around a resonance dip at 293 THz in full-wave simulation result (symbols). By fitting the simulation results, we have also adopted a coupled-mode theory, shown as solid lines with excellent agreement. The coupled-mode theory models the scattering of the metasurface by the vertical gold bars as two resonating electric dipole modes, with coupling controlled by h , resonating frequencies controlled by w_i and l_i , and resonating linewidth fine-tuned by l_i . The various parameters of the coupled-mode model are then obtained by fitting the scattering parameters in the whole relevant phase space [Fig. 3(a)] (see Appendix D for details). We note that there is another resonance dip at around 400 THz without the UZR effect, which serves as a comparison in considering the quantum interference below.

The scattering matrix of a UZR metasurface $S = \begin{pmatrix} t & 0 \\ r & t \end{pmatrix}$ has to be nonunitary (r here means forward complex reflection amplitude). Here, we adopt the ancilla-mode formulation in which the 2×2 S matrix with material loss will need at most 2 ancilla modes to expand it into a unitary one [39,40]. The two ancilla modes correspond to the two loss channels of the metamaterial atoms. To achieve the proposed effect, we find that only one loss channel is needed (see Appendix B for details). It means an eigenvalue of $S^\dagger S$ becomes one. This is called the single ancilla-mode condition here and is found to be

$$|t|^2 = 1 - |r|. \quad (1)$$

In this case, we expand S into a 3×3 unitary S' matrix with one ancilla mode (the third index for the loss channel) as

$$S' = \begin{pmatrix} t & 0 & -r^*t^2/(|t|^2\sqrt{|r|}) \\ r & t & t\sqrt{|r|} \\ t^*r/\sqrt{|r|} & -\sqrt{|r|} & |t|^2 \end{pmatrix}, \quad (2)$$

which is obtained through a singular value decomposition with the compositing diagonal matrix being modified through the extent of loss in each ancilla mode (see Appendix B for details). Such kind of linear input-output relations can also be deduced from the system-and-bath Hamiltonian if the full dynamics of the modes on the metasurfaces are known [41,42]. Now, we consider the quantum interference of a $|11\rangle$ input to the metasurface (a pair of indistinguishable photons entering each side). By using Eq. (2), we have

$$\begin{aligned} |11\rangle &= \hat{a}_1^\dagger \hat{a}_2^\dagger |0\rangle \\ &\rightarrow (t\hat{b}_1^\dagger + r\hat{b}_2^\dagger + t^*|r|^{-1/2}r\hat{b}_3^\dagger)(t\hat{b}_2^\dagger - |r|^{1/2}\hat{b}_3^\dagger)|0\rangle, \end{aligned}$$

where \hat{a}_i^\dagger (\hat{b}_i^\dagger) is the photon creation operation for port i at input (output). For a clearer notation, we add a third index in the ‘‘ket’’ to indicate the number of photon going into the loss channel. After expanding out the product terms, we obtain the final state as

$$\begin{aligned} |110\rangle &\rightarrow (|t|^2 - |r|)|r|^{-1/2}r|011\rangle \\ &\quad - \sqrt{2}t^*r|002\rangle - |r|^{1/2}t|101\rangle + t^2|110\rangle + \sqrt{2}tr|020\rangle. \end{aligned}$$

The first term accounts for the quantum interference for output $|01\rangle$ whereas we can see no interference in the third term for $|10\rangle$ output. In fact, for the single-photon output state $|10\rangle$, there is only one process (the photon from port 1

is transmitted and the photon from port 2 is absorbed) since $r_b = 0$ and thus no quantum interference occurs. On the other hand, there are two processes that can contribute to the single-photon output state $|01\rangle$. In the first case, the photon from port 2 is transmitted (t) while the photon from port 1 is absorbed ($t^*|r|^{-1/2}r$). As for the second case the photon from port 1 is reflected (r) while the photon from port 2 is absorbed ($-|r|^{1/2}$). These two processes cannot be distinguished and thus they can interfere with each other (with result $\propto |t|^2 - |r|$). Furthermore, to obtain destructive quantum interference, we solve $|t|^2 - |r| = 0$, together with the single ancilla-mode condition Eq. (1). The condition of one-sided destructive quantum interference becomes

$$|t| = 1/\sqrt{2}, \quad |r| = 1/2. \quad (3)$$

For general nonunitary scattering matrices (with only losses) other than the above values, the probabilities for the different single and two-photons output states can be evaluated similarly with a formulation of two-ancilla modes:

$$\begin{aligned} P_Q(0, 1) &= P_C(0, 1) - t_f^*t_b^*r_f r_b \\ &\quad - t_f t_b r_f^* r_b^* - 2|t_b|^2|r_f|^2, \end{aligned} \quad (4)$$

$$\begin{aligned} P_Q(1, 0) &= P_C(1, 0) - t_f^*t_b^*r_f r_b \\ &\quad - t_f t_b r_f^* r_b^* - 2|t_f|^2|r_b|^2, \end{aligned} \quad (5)$$

$$P_Q(0, 2) = P_C(0, 2) + |t_b|^2|r_f|^2, \quad (6)$$

$$P_Q(1, 1) = P_C(1, 1) + t_f^*t_b^*r_f r_b + t_f t_b r_f^* r_b^*, \quad (7)$$

$$P_Q(2, 0) = P_C(2, 0) + |t_f|^2|r_b|^2. \quad (8)$$

The first (second) slot for the probability functions indicates the number of photons in port 1(2) and the subscript ‘‘C’’ indicates the classical probabilities, which assumes the input photons are distinguishable and undergo a probabilistic process acting like bullets [43]. The difference to their classical counterparts, e.g., $P_C(0, 1) = |t_b|^2A_f + |r_f|^2A_b$ and $P_C(1, 0) = |r_b|^2A_f + |t_f|^2A_b$ for the single-photon output states, where A_f and A_b are absorption coefficients in the forward and backward directions respectively, contributes to quantum interference. When $r_b = 0$, the quantum interference in $P_Q(1, 0)$ is turned off and $P_Q(1, 0)$ is equal to its classical counterpart while quantum interference still exists in $P_Q(0, 1)$.

From the spectra shown in Fig. 3(b), we calculate quantum probabilities for different outputs from $|11\rangle$ input, as well as the classical probabilities. Figure 4(a) shows the probabilities for $|10\rangle$ and $|01\rangle$ outputs (symbols for results calculated from full-wave simulation and lines from coupled mode model). At the UZR point (dashed line at 293 THz), $P_Q(1, 0)$ is equal to $P_C(1, 0)$ indicating the disappearance of quantum interference on the reflectionless side [shown in Fig. 4(a) inset]. On the other hand, $P_Q(0, 1)$ and $P_C(0, 1)$ differ a lot. For a system with loss, $P_C(0, 1)$ for the $|11\rangle$ input state is nonzero. With the quantum interference, $P_Q(0, 1)$ becomes smaller than $P_C(0, 1)$ and the designed destructive quantum interference further eliminates the $|01\rangle$ output with $P_Q(0, 1)/P_C(0, 1) \approx 0.058$. It is noted that the current example [in Fig. 3(b)] approaches the one-sided destructive quantum interference condition Eq. (3)

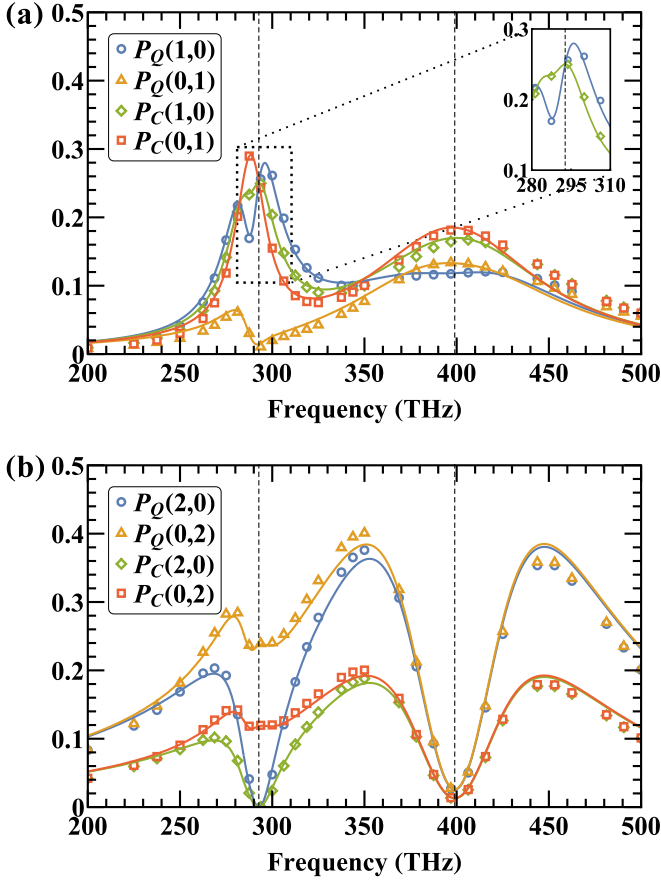


FIG. 4. The classical and quantum probabilities for output states (a) with only one output photon and (b) with two output photons from $|11\rangle$ input at different frequencies. Vertical dashed lines denote the resonance frequencies shown in Fig. 3(b).

with zero r_b . In essence, the design is achieved by choosing appropriate values for w_1 and h to satisfy Eq. (3) and l_1 is then chosen to have the appropriate level of loss contrast to match the coupling between two gold bars to get an exceptional point (UZR). On the contrary, at another resonance around 400 THz, Eq. (3) is not satisfied and the probabilities for $|01\rangle$ and $|10\rangle$, no matter quantum or classical, are in the similar scale. Figure 4(b) shows the probabilities for output states $|20\rangle$ and $|02\rangle$ for the same input $|11\rangle$. At UZR, the probability for output $|20\rangle$ reaches zero since the backward incident photon cannot be reflected. On the other hand, the quantum probability for $|02\rangle$ differs from its classical counterparts by exactly a factor of 2, resulting from the quantum effect by mutual stimulation of two photons in the same state [44].

In principle, the proposed one-sided destructive quantum interference can be implemented with conventional optical elements. Using singular value decomposition, we can decompose any scattering matrix satisfying Eq. (3) with zero r_b : $S = \frac{1}{2} \begin{pmatrix} \sqrt{2}e^{i\phi_1} & 0 \\ e^{i\phi_2} & \sqrt{2}e^{i\phi_1} \end{pmatrix}$ with arbitrary ϕ_1 and ϕ_2 into two unitary matrices and a diagonal matrix denoting loss (see Appendix C for details). Such a decomposition corresponds to the implementation in Fig. 5, the beam splitter (BS) 1 and 3 are two one-third BS corresponding to the two unitary matrices. The BS 2 is a 25:75 BS to introduce loss by interfering with ancilla

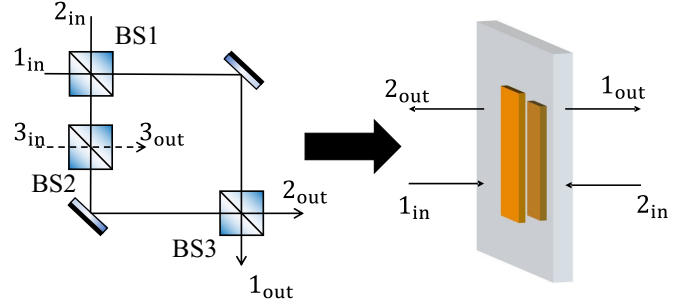


FIG. 5. Simplifying one-sided destructive quantum interference from the scheme using beam splitters (BSs) to our designed metasurfaces. BS 1 and 3 are one-third BS while BS 2 is a 25:75 BS to introduce loss in channel 2 with vacuum mode 3.

vacuum state 3, while there is no loss in another channel thus no BS in this arm. While this decomposition into conventional optical elements can be used to realize the proposed one-sided destructive quantum interference, the tailor-made metasurface provides a more compact platform with subwavelength thickness and greatly simplifies the setup.

III. CONCLUSION

In conclusion, we have proposed one-sided destructive quantum interference effect based on a lossy metasurface with UZR at an exceptional point. When two indistinguishable photons enter both sides of the metasurface, the quantum interference to the single photon output state on the reflectionless side is turned off while the quantum interference to the single photon output state on the other side can be tuned through two indistinguishable processes. Such one-sided quantum interference can be further made totally destructive with a 50:25:0 beam-splitting ratio in percentage among the transmission and the two reflection efficiencies. Our investigation allows metasurfaces to become a versatile platform to control quantum interference with the additional degrees of freedom from material loss and non-Hermitian exceptional point. It also allows construction of entangled states with elimination of certain states through both quantum interference and UZR effect, indicating potential applications in quantum state preparation and quantum information processing with elements of subwavelength thickness.

ACKNOWLEDGMENTS

The work was supported by the Research Grants Council of Hong Kong (Projects No. C6013-18G, No. 16304020, No. 16304520, No. AoE/P-502/20) and by the Croucher Foundation.

APPENDIX A: OUTPUT PROBABILITIES FOR $|11\rangle$ INPUT

For $|11\rangle$ input in a passive metasurface with scattering matrix $S = \begin{pmatrix} r_f & r_b \\ r_f & t_b \end{pmatrix}$, classical probabilities can be calculated assuming that the two photons are distinguishable particles and undergo independent probabilistic processes acting like

bullets, the results are

$$P_C(1, 1) = |t_f|^2 |t_b|^2 + |r_f|^2 |r_b|^2, \quad (\text{A1})$$

$$P_C(0, 2) = |r_f|^2 |t_b|^2, \quad (\text{A2})$$

$$P_C(2, 0) = |t_f|^2 |r_b|^2, \quad (\text{A3})$$

$$P_C(0, 1) = |t_b|^2 (1 - |t_f|^2 - |r_f|^2) + |r_f|^2 (1 - |t_b|^2 - |r_b|^2), \quad (\text{A4})$$

$$P_C(1, 0) = |r_b|^2 (1 - |t_f|^2 - |r_f|^2) + |t_f|^2 (1 - |t_b|^2 - |r_b|^2). \quad (\text{A5})$$

The quantum probabilities can be calculated from full ancilla mode method [40] or noise operator formalism [33,44]. The results are listed in terms of classical probabilities,

$$P_Q(1, 1) = P_C(1, 1) + t_f^* t_b^* r_f r_b + t_f t_b r_f^* r_b^*, \quad (\text{A6})$$

$$P_Q(0, 1) = P_C(0, 1) - t_f^* t_b^* r_f r_b - t_f t_b r_f^* r_b^* - 2|t_b|^2 |r_f|^2, \quad (\text{A7})$$

$$P_Q(1, 0) = P_C(1, 0) - t_f^* t_b^* r_f r_b - t_f t_b r_f^* r_b^* - 2|t_f|^2 |r_b|^2, \quad (\text{A8})$$

$$P_Q(0, 2) = P_C(0, 2) + |t_b|^2 |r_f|^2, \quad (\text{A9})$$

$$P_Q(2, 0) = P_C(2, 0) + |t_f|^2 |r_b|^2. \quad (\text{A10})$$

One can find these expressions in [44] by taking the overlap integral to be 1, which assumes that the two photons are indistinguishable.

APPENDIX B: ANCILLA MODE FORMALISM TO INCLUDE ONE LOSS CHANNEL

For reciprocal metasurfaces with unidirectional zero backward reflection, the scattering matrix can be written as

$$S = \begin{pmatrix} t & 0 \\ r & t \end{pmatrix}. \quad (\text{B1})$$

Since only loss occurs on the metasurface, we should have that all eigenvalues of $S^\dagger S$ are less than or equal to 1 [43]. We take the larger eigenvalue $\lambda_1 = \frac{1}{4}(|r| + \sqrt{|r|^2 + 4|t|^2})^2 \leq 1$, and get

$$|r| + |t|^2 \leq 1.$$

Furthermore, for the proposed one-sided destructive quantum interference, we require $P_Q(0, 1) = 0$. By taking $t_f = t_b = t$, $r_f = r$, and $r_b = 0$ [in Eq. (A7)], we get the inequality for $P_Q(0, 1)$,

$$\begin{aligned} P_Q(0, 1) &= |t|^2 - |t|^4 + |r|^2 (1 - 4|t|^2) \\ &\geq |t|^2 - |t|^4 + (1 - |t|^2)^2 (1 - 4|t|^2) \\ &= (1 - 2|t|^2)^2 (1 - |t|^2). \end{aligned}$$

From this inequality, $P_Q(0, 1) = 0$ only happens when

$$|r| + |t|^2 = 1, \quad (\text{B2})$$

$$1 - 2|t|^2 = 0 \quad (\text{B3})$$

(apart from the trivial vacuum case $|t| = 1$ and $|r| = 0$).

The scattering matrix for one-sided destructive quantum interference is obtained as

$$|t| = 1/\sqrt{2}, \quad |r| = 1/2.$$

It is noted that when Eq. (B2) is fulfilled, an eigenvalue of $S^\dagger S$ becomes 1. This is called the single ancilla mode condition here since there exists a coherent input with no absorption. We note that the single ancilla mode condition is necessarily true at one-sided quantum destructive interference.

To further explore the quantum interference effect with loss, we adopt the ancilla-mode formalism with single ancilla mode condition to find the state transformation [40]. We use singular value decomposition to decompose the $S = UDW$, in which

$$U = \begin{pmatrix} \frac{t^2 r^*}{|r||t|\sqrt{1+|t|^2}} & -\frac{t^2 r^*}{|r||t|^2\sqrt{1+|t|^2}} \\ \frac{|t|\sqrt{1+|t|^2}}{|r|\sqrt{1+|t|^2}} & \frac{t}{\sqrt{1+|t|^2}} \end{pmatrix}, \quad (\text{B4})$$

$$D = \begin{pmatrix} 1 & 0 \\ 0 & |t|^2 \end{pmatrix}, \quad (\text{B5})$$

$$W = \begin{pmatrix} \frac{t^* r}{|r||t|\sqrt{1+|t|^2}} & \frac{|t|}{\sqrt{1+|t|^2}} \\ -\frac{t^* r}{|r|\sqrt{1+|t|^2}} & \frac{1}{\sqrt{1+|t|^2}} \end{pmatrix}, \quad (\text{B6})$$

where matrix U and W are unitary matrix and D is a diagonal matrix with singular value, characterizing the loss in the channels. One can easily check that

$$UDW = \begin{pmatrix} t & 0 \\ r(1-|t|^2) & t \end{pmatrix}.$$

Then, with single ancilla-mode condition Eq. (A2), the above matrix returns to the original S [Eq. (A1)].

According to the recipe in the ancilla-mode formulation, we expand the D matrix with beam-splitter-like transformation to include the loss channels (at most two channels), while the U and W matrices can be expanded appropriately with identity matrix as a subblock,

$$U' = \begin{pmatrix} \frac{t^2 r^*}{|r||t|\sqrt{1+|t|^2}} & -\frac{t^2 r^*}{|r||t|^2\sqrt{1+|t|^2}} & 0 & 0 \\ \frac{|t|\sqrt{1+|t|^2}}{|r|\sqrt{1+|t|^2}} & \frac{t}{\sqrt{1+|t|^2}} & 0 & 0 \\ 0 & 0 & 1 & 0 \\ 0 & 0 & 0 & 1 \end{pmatrix}, \quad (\text{B7})$$

$$D' = \begin{pmatrix} 1 & 0 & 0 & 0 \\ 0 & |t|^2 & \sqrt{1-|t|^4} & 0 \\ 0 & -\sqrt{1-|t|^4} & |t|^2 & 0 \\ 0 & 0 & 0 & 1 \end{pmatrix}, \quad (\text{B8})$$

$$W' = \begin{pmatrix} \frac{t^* r}{|r||t|\sqrt{1+|t|^2}} & \frac{|t|}{\sqrt{1+|t|^2}} & 0 & 0 \\ -\frac{t^* r}{|r|\sqrt{1+|t|^2}} & \frac{1}{\sqrt{1+|t|^2}} & 0 & 0 \\ 0 & 0 & 1 & 0 \\ 0 & 0 & 0 & 1 \end{pmatrix}. \quad (\text{B9})$$

Then the expanded $S' = U'D'W'$ matrix becomes unitary, with the third and fourth index now representing the loss channels,

$$S' = U'D'W' = \begin{pmatrix} t & 0 & -r^*t^2/(|t|^2\sqrt{|r|}) & 0 \\ r & t & t\sqrt{|r|} & 0 \\ t^*r/\sqrt{|r|} & -\sqrt{|r|} & |t|^2 & 0 \\ 0 & 0 & 0 & 1 \end{pmatrix}. \quad (\text{B10})$$

It is noted that although two loss channels are included in the formulation, only one is coupled to the input modes while the other one is not. It is actually resulting from the presence of a unit singular value in Eq. (B5). It also means an eigenvalue of $S^\dagger S$ becomes 1 and then there is a coherent input wave ($\phi = (|r|, t^*r)^T$) with no absorption for the system, i.e., $\phi^\dagger S^\dagger S \phi = \phi^\dagger \phi$. We can rewrite the matrix by removing the decoupled loss channel, giving the matrix used in text,

$$S' = \begin{pmatrix} t & 0 & -r^*t^2/(|t|^2\sqrt{|r|}) \\ r & t & t\sqrt{|r|} \\ t^*r/\sqrt{|r|} & -\sqrt{|r|} & |t|^2 \end{pmatrix}. \quad (\text{B11})$$

The input modes operators (\hat{a}_i^\dagger) can be written as combination of output operators (\hat{b}_i^\dagger), $\hat{a}_i^\dagger \rightarrow \sum_{ij} S_{ij}^T \hat{b}_j^\dagger$. With this relation, we can find the output state for input state $|11\rangle$

$$\begin{aligned} |11\rangle &= \hat{a}_1^\dagger \hat{a}_2^\dagger |0\rangle \\ &\rightarrow (t\hat{b}_1^\dagger + r\hat{b}_2^\dagger + t^*|r|^{-1/2}r\hat{b}_3^\dagger)(t\hat{b}_2^\dagger - |r|^{1/2}\hat{b}_3^\dagger)|0\rangle. \end{aligned}$$

We can add a third index in the ket to indicate the number of photons in the loss channel, giving the transformation in Fock state,

$$\begin{aligned} |110\rangle &\rightarrow (|t|^2 - |r|)|r|^{-1/2}r|011\rangle - \sqrt{2}t^*r|002\rangle \\ &\quad - |r|^{1/2}t|101\rangle + t^2|110\rangle + \sqrt{2}tr|020\rangle. \end{aligned}$$

From the output state, we can further find the probabilities for different outputs,

$$\begin{aligned} P_Q(1, 1) &= |t|^4 = P_C(1, 1), \\ P_Q(0, 1) &= (|t|^2 - |r|)^2|r| = P_C(0, 1) - 2|t|^2|r|^2, \\ P_Q(1, 0) &= |r||t|^2 = |t|^2(1 - |t|^2) = P_C(1, 0), \\ P_Q(0, 2) &= 2|t|^2|r|^2 = P_C(0, 2) + |t|^2|r|^2, \\ P_Q(2, 0) &= 0 = P_C(2, 0), \end{aligned}$$

which can be checked using expressions for general cases Eqs. (A6)–(A10) with Eq. (B2) and the scattering matrix being Eq. (B1). It constitutes a special case for Eqs. (4)–(8) in the main text.

APPENDIX C: IMPLEMENTATION OF THE PROPOSED MATRIX

The proposed one-sided destructive quantum interference effect can be implemented with the scattering matrix $S = \frac{1}{2} \begin{pmatrix} \sqrt{2}e^{i\phi_1} & 0 \\ e^{i\phi_2} & \sqrt{2}e^{i\phi_1} \end{pmatrix}$ with arbitrary ϕ_1 and ϕ_2 . This matrix can be first transferred into a real matrix with only magnitude infor-

mation using phase shifters on separate ports, whose matrix representations are

$$PS_1(\theta) = \begin{pmatrix} e^{i\theta} & 0 \\ 0 & 1 \end{pmatrix}, \quad (\text{C1})$$

$$PS_2(\theta) = \begin{pmatrix} 1 & 0 \\ 0 & e^{i\theta} \end{pmatrix}, \quad (\text{C2})$$

where the subscript denotes the port number. Then the original scattering matrix can be turned into purely real

$$\begin{aligned} S_{re} &= PS_1(-\phi_1)PS_2(-\phi_1)S PS_2(\phi_2 - \phi_1) \\ &= \frac{1}{2} \begin{pmatrix} \sqrt{2} & 0 \\ 1 & \sqrt{2} \end{pmatrix}. \end{aligned} \quad (\text{C3})$$

It is worthwhile to note that for $|11\rangle$ input and our interested output $|01\rangle$, the phase shifters would not change the states. Therefore, we focus on the implementation of the S_{re} , which can be decomposed into three matrices as $S_{re} = UDW$, in which

$$U = \frac{1}{\sqrt{3}} \begin{pmatrix} 1 & -\sqrt{2} \\ \sqrt{2} & 1 \end{pmatrix}, \quad (\text{C4})$$

$$D = \begin{pmatrix} 1 & 0 \\ 0 & \frac{1}{2} \end{pmatrix}, \quad (\text{C5})$$

$$W = \frac{1}{\sqrt{3}} \begin{pmatrix} \sqrt{2} & 1 \\ -1 & \sqrt{2} \end{pmatrix}, \quad (\text{C6})$$

where the matrix U and W are a unitary matrix and can be implemented with one-third beam splitters and D is a diagonal matrix characterizing the loss in the channels. The one loss channel can be implemented with 25:75 BS and interference with an ancilla vacuum mode as represented by the expanded 3×3 matrix D' form D , while the matrices U and W can be expanded respectively to U' and W' ,

$$U' = \begin{pmatrix} 1/\sqrt{3} & -\sqrt{2}/\sqrt{3} & 0 \\ \sqrt{2}/\sqrt{3} & 1/\sqrt{3} & 0 \\ 0 & 0 & 1 \end{pmatrix}, \quad (\text{C7})$$

$$D' = \begin{pmatrix} 1 & 0 & 0 \\ 0 & \frac{1}{2} & \frac{\sqrt{3}}{2} \\ 0 & -\frac{\sqrt{3}}{2} & \frac{1}{2} \end{pmatrix}, \quad (\text{C8})$$

$$W' = \begin{pmatrix} \sqrt{2}/\sqrt{3} & 1/\sqrt{3} & 0 \\ -1/\sqrt{3} & \sqrt{2}/\sqrt{3} & 0 \\ 0 & 0 & 1 \end{pmatrix}, \quad (\text{C9})$$

and the corresponding 3×3 unitary matrix for the whole system is

$$S' = U'D'W' = \frac{1}{2} \begin{pmatrix} \sqrt{2} & 0 & -\sqrt{2} \\ 1 & \sqrt{2} & 1 \\ 1 & -\sqrt{2} & 1 \end{pmatrix}. \quad (\text{C10})$$

APPENDIX D: COUPLED-MODE THEORY

We use coupled-mode theory (CMT) to explain the simulation results and find the 2×2 scattering matrix $S = \{\{t_f, r_b\}, \{r_f, t_b\}\}$ for y -polarization light. In this model, we

assume two electric dipole modes on the two gold bars respectively and take the middle plane of the two gold bars as reference. The matrix to convert input field into local field can be written

$$A = \begin{pmatrix} e^{-i\phi_s/2} & e^{i\phi_s/2} \\ e^{i\phi_s/2} & e^{-i\phi_s/2} \end{pmatrix}, \quad (\text{D1})$$

in which ϕ_s is the phase difference resulting from the light propagation in between the two antennas and thus linear to the separation of the two strips. The matrix

$$\Lambda_a = \begin{pmatrix} \frac{f-f_1}{a_1} & \kappa \\ \kappa & \frac{f-f_2}{a_2} \end{pmatrix} + \begin{pmatrix} i\gamma_1 & 0 \\ 0 & i\gamma_2 \end{pmatrix} \quad (\text{D2})$$

is used to transform the local field to the resonance modes, in which f_i , a_i , and γ_i describe the resonance frequency, resonance strength, and decay rate of the resonance modes. In this way, we can write down the resonance modes as

$$p = -(\Lambda_a + i\Gamma_s)^{-1} A \mathbf{E}_{\text{in}}, \quad (\text{D3})$$

where $\mathbf{E}_{\text{in}} = [\mathbf{E}_{1,\text{in}}, \mathbf{E}_{2,\text{in}}]^T$ describes the amplitude of the input field, $\Gamma_s = AA^\dagger/2$ describes the radiative scattering [45], and $\mathbf{p} = [p_1, p_2]^T$ describes the resonance modes. The outgoing waves are

$$\begin{aligned} \mathbf{E}_{\text{out}} &= \mathbf{E}_{\text{in}} + iA^\dagger p \\ &= \mathbf{E}_{\text{in}} - iA^\dagger (\Lambda_a + i\Gamma_s)^{-1} A \mathbf{E}_{\text{in}}, \end{aligned} \quad (\text{D4})$$

Therefore, the scattering matrix takes the form

$$S = I - iA^\dagger (\Lambda_a + i\Gamma_s)^{-1} A. \quad (\text{D5})$$

We simulated multiple configurations with varying w_1 , l_1 , and h , and fitted the parameters in CMT with the geometric parameters. In the parameter space, we found the fitted relation to be

$$\begin{aligned} f_1 &= 424.4 + 0.81h - 0.90l_1 + 0.62w_1, \\ a_1 &= 46 - 0.32h - 0.16l_1 + 0.15w_1, \\ \gamma_1 &= 2.94 - 0.011l_1 - 0.006w_1, \\ f_2 &= 290.5 + 7.81h - 0.17h^2, \\ a_2 &= 14 + 0.78h - 0.011h^2, \\ \gamma_2 &= 0.27, \\ \kappa &= -4.69 + 0.23h - 0.004h^2, \\ s &= 25.7 + 0.88h, \end{aligned}$$

in which the dimensions are in unit nm, $f_1, f_2, \gamma_1, \gamma_2$, and κ are in unit THz, and s is in unit nm, connecting to ϕ_s with $\phi_s = \frac{\pi fs}{c}$, in which f is the frequency of wave and c is the speed of light. With the parameter fitting, the family of UZR cases is estimated and shown in Fig. 3(a). We note that from the fitting, we have found that there are additional dependencies on the separation h in f_1, f_2, a_1 , and a_2 as our CMT is effectively a two-mode model, so that all the other coupling terms to other modes are lumped into these terms as perturbation.

-
- [1] N. Yu, P. Genevet, M. A. Kats, F. Aieta, J.-P. Tetienne, F. Capasso, and Z. Gaburro, Light propagation with phase discontinuities: Generalized laws of reflection and refraction, *Science* **334**, 333 (2011).
- [2] M. Khorasaninejad, W. T. Chen, R. C. Devlin, J. Oh, A. Y. Zhu, and F. Capasso, Metalenses at visible wavelengths: Diffraction-limited focusing and subwavelength resolution imaging, *Science* **352**, 1190 (2016).
- [3] G. Zheng, H. Mühlenbernd, M. Kenney, G. Li, T. Zentgraf, and S. Zhang, Metasurface holograms reaching 80% efficiency, *Nat. Nanotechnol.* **10**, 308 (2015).
- [4] M. A. Gorlach, X. Ni, D. A. Smirnova, D. Korobkin, D. Zhirihin, A. P. Slobozhanyuk, P. A. Belov, A. Alù, and A. B. Khanikaev, Far-field probing of leaky topological states in all-dielectric metasurfaces, *Nat. Commun.* **9**, 909 (2018).
- [5] A. Slobozhanyuk, A. V. Shchelokova, X. Ni, S. Hossein Mousavi, D. A. Smirnova, P. A. Belov, A. Alù, Y. S. Kivshar, and A. B. Khanikaev, Near-field imaging of spin-locked edge states in all-dielectric topological metasurfaces, *Appl. Phys. Lett.* **114**, 031103 (2019).
- [6] C. M. Bender and S. Boettcher, Real Spectra in Non-Hermitian Hamiltonians Having PT Symmetry, *Phys. Rev. Lett.* **80**, 5243 (1998).
- [7] C. M. Bender, M. V. Berry, and A. Mandilara, Generalized PT symmetry and real spectra, *J. Phys. A: Math. Gen.* **35**, L467 (2002).
- [8] A. Guo, G. J. Salamo, D. Duchesne, R. Morandotti, M. Volatier-Ravat, V. Aimez, G. A. Siviloglou, and D. N. Christodoulides, Observation of PT-Symmetry Breaking in Complex Optical Potentials, *Phys. Rev. Lett.* **103**, 093902 (2009).
- [9] Z. Lin, H. Ramezani, T. Eichelkraut, T. Kottos, H. Cao, and D. N. Christodoulides, Unidirectional Invisibility Induced by PT-Symmetric Periodic Structures, *Phys. Rev. Lett.* **106**, 213901 (2011).
- [10] W. Chen, Ş. Kaya Özdemir, G. Zhao, J. Wiersig, and L. Yang, Exceptional points enhance sensing in an optical microcavity, *Nature (London)* **548**, 192 (2017).
- [11] B. Peng, Ş. K. Özdemir, S. Rotter, H. Yilmaz, M. Liertzer, F. Monifi, C. M. Bender, F. Nori, and L. Yang, Loss-induced suppression and revival of lasing, *Science* **346**, 328 (2014).
- [12] M. Lawrence, N. Xu, X. Zhang, L. Cong, J. Han, W. Zhang, and S. Zhang, Manifestation of PT Symmetry Breaking in Polarization Space with Terahertz Metasurfaces, *Phys. Rev. Lett.* **113**, 093901 (2014).
- [13] Y. Sun, W. Tan, H. Q. Li, J. Li, and H. Chen, Experimental Demonstration of a Coherent Perfect Absorber with PT Phase Transition, *Phys. Rev. Lett.* **112**, 143903 (2014).
- [14] J.-H. Park, A. Ndao, W. Cai, L. Hsu, A. Kodigala, T. Lepetit, Y.-H. Lo, and B. Kanté, Symmetry-breaking-induced plasmonic exceptional points and nanoscale sensing, *Nat. Phys.* **16**, 462 (2020).
- [15] A. Tuniz, T. Wieduwilt, and M. A. Schmidt, Tuning the Effective PT Phase of Plasmonic Eigenmodes, *Phys. Rev. Lett.* **123**, 213903 (2019).
- [16] H. M. Leung, W. Gao, R. Zhang, R. Zhang, Q. Zhao, X. Wang, C. T. Chan, J. Li, J. Li, W. Y. Tam, and W. Y. Tam, Exceptional

- point-based plasmonic metasurfaces for vortex beam generation, *Opt. Express* **28**, 503 (2020).
- [17] L. Feng, Y.-L. Xu, W. S. Fegadolli, M.-H. Lu, J. E. B. Oliveira, V. R. Almeida, Y.-F. Chen, and A. Scherer, Experimental demonstration of a unidirectional reflectionless parity-time metamaterial at optical frequencies, *Nat. Mater.* **12**, 108 (2013).
- [18] J. Gear, Y. Sun, S. Xiao, L. Zhang, R. Fitzgerald, S. Rotter, H. Chen, and J. Li, Unidirectional zero reflection as gauged parity-time symmetry, *New J. Phys.* **19**, 123041 (2017).
- [19] K. Wang, J. G. Titchener, S. S. Kruk, L. Xu, H.-P. Chung, M. Parry, I. I. Kravchenko, Y.-H. Chen, A. S. Solntsev, Y. S. Kivshar, D. N. Neshev, and A. A. Sukhorukov, Quantum metasurface for multiphoton interference and state reconstruction, *Science* **361**, 1104 (2018).
- [20] T. Stav, A. Faerman, E. Maguid, D. Oren, V. Kleiner, E. Hasman, and M. Segev, Quantum entanglement of the spin and orbital angular momentum of photons using metamaterials, *Science* **361**, 1101 (2018).
- [21] L. Li, Z. Liu, X. Ren, S. Wang, V.-C. Su, M.-K. Chen, C. H. Chu, H. Y. Kuo, B. Liu, W. Zang, G. Guo, L. Zhang, Z. Wang, S. Zhu, and D. P. Tsai, Metalens-array-based high-dimensional and multiphoton quantum source, *Science* **368**, 1487 (2020).
- [22] P. K. Jha, N. Shitrit, J. Kim, X. Ren, Y. Wang, and X. Zhang, Metasurface-mediated quantum entanglement, *ACS Photonics* **5**, 971 (2018).
- [23] E. Knill, R. Laflamme, and G. J. Milburn, A scheme for efficient quantum computation with linear optics, *Nature (London)* **409**, 46 (2001).
- [24] N. Gisin and R. Thew, Quantum communication, *Nat. Photonics* **1**, 165 (2007).
- [25] J. L. O'Brien, Optical quantum computing, *Science* **318**, 1567 (2007).
- [26] A. Aspuru-Guzik and P. Walther, Photonic quantum simulators, *Nat. Phys.* **8**, 285 (2012).
- [27] M. Kang, K. M. Lau, T. K. Yung, S. Du, W. Y. Tam, and J. Li, Tailor-made unitary operations using dielectric metasurfaces, *Opt. Express* **29**, 5677 (2021).
- [28] Q. Li, W. Bao, Z. Nie, Y. Xia, Y. Xue, Y. Wang, S. Yang, and X. Zhang, A non-unitary metasurface enables continuous control of quantum photon-photon interactions from bosonic to fermionic, *Nat. Photonics* **15**, 267 (2021).
- [29] L. Xiao, X. Zhan, Z. H. Bian, K. K. Wang, X. Zhang, X. P. Wang, J. Li, K. Mochizuki, D. Kim, N. Kawakami, W. Yi, H. Obuse, B. C. Sanders, and P. Xue, Observation of topological edge states in parity-time-symmetric quantum walks, *Nat. Phys.* **13**, 1117 (2017).
- [30] L. Xiao, K. Wang, X. Zhan, Z. Bian, K. Kawabata, M. Ueda, W. Yi, and P. Xue, Observation of Critical Phenomena in Parity-Time-Symmetric Quantum Dynamics, *Phys. Rev. Lett.* **123**, 230401 (2019).
- [31] F. E. Öztürk, T. Lappe, G. Hellmann, J. Schmitt, J. Klaers, F. Vewinger, J. Kroha, and M. Weitz, Observation of a non-Hermitian phase transition in an optical quantum gas, *Science* **372**, 88 (2021).
- [32] C. K. Hong, Z. Y. Ou, and L. Mandel, Measurement of Subpicosecond Time Intervals between Two Photons by Interference, *Phys. Rev. Lett.* **59**, 2044 (1987).
- [33] S. M. Barnett, J. Jeffers, A. Gatti, and R. Loudon, Quantum optics of lossy beam splitters, *Phys. Rev. A* **57**, 2134 (1998).
- [34] J. Jeffers, Interference and the lossless lossy beam splitter, *J. Mod. Opt.* **47**, 1819 (2000).
- [35] S. Huang and G. S. Agarwal, Coherent perfect absorption of path entangled single photons, *Opt. Express* **22**, 20936 (2014).
- [36] T. Roger, S. Vezzoli, E. Bolduc, J. Valente, J. J. F. Heitz, J. Jeffers, C. Soci, J. Leach, C. Couteau, N. I. Zheludev, and D. Faccio, Coherent perfect absorption in deeply subwavelength films in the single-photon regime, *Nat. Commun.* **6**, 7031 (2015).
- [37] T. Roger, S. Restuccia, A. Lyons, D. Giovannini, J. Romero, J. Jeffers, M. Padgett, and D. Faccio, Coherent Absorption of NOON States, *Phys. Rev. Lett.* **117**, 023601 (2016).
- [38] B. Vest, M.-C. Dheur, É. Devaux, A. Baron, E. Rousseau, J.-P. Hugonin, J.-J. Greffet, G. Messin, and F. Marquier, Anticoalescence of bosons on a lossy beam splitter, *Science* **356**, 1373 (2017).
- [39] N. Tischler, C. Rockstuhl, and K. Słowik, Quantum Optical Realization of Arbitrary Linear Transformations Allowing for Loss and Gain, *Phys. Rev. X* **8**, 021017 (2018).
- [40] L. Knöll, S. Scheel, E. Schmidt, D.-G. Welsch, and A. V. Chizhov, Quantum-state transformation by dispersive and absorbing four-port devices, *Phys. Rev. A* **59**, 4716 (1999).
- [41] C. W. Gardiner and M. J. Collett, Input and output in damped quantum systems: Quantum stochastic differential equations and the master equation, *Phys. Rev. A* **31**, 3761 (1985).
- [42] C. Viviescas and G. Hackenbroich, Field quantization for open optical cavities, *Phys. Rev. A* **67**, 013805 (2003).
- [43] R. Uppu, T. A. Wolterink, T. B. Trentup, and P. W. Pinkse, Quantum optics of lossy asymmetric beam splitters, *Opt. Express* **24**, 16440 (2016).
- [44] R. Lange, J. Brendel, E. Mohler, and W. Martienssen, Beam splitting experiments with classical and with quantum particles, *Europhys. Lett.* **5**, 619 (1988).
- [45] W. Suh, Z. Wang, and S. Fan, Temporal coupled-mode theory and the presence of non-orthogonal modes in lossless multi-mode cavities, *IEEE J. Quantum Electron.* **40**, 1511 (2004).